

Pat1 protects centromere-specific histone H3 variant Cse4 from Psh1-mediated ubiquitination

Prashant K. Mishra^a, Jiasheng Guo^b, Lauren E. Dittman^a, Julian Haase^b, Elaine Yeh^b, Kerry Bloom^b, and Munira A. Basrai^a

^aGenetics Branch, National Cancer Institute, National Institutes of Health, Bethesda, MD 20892; ^bDepartment of Biology, University of North Carolina, Chapel Hill, NC 27599

ABSTRACT Evolutionarily conserved histone H3 variant Cse4 and its homologues are essential components of specialized centromere (*CEN*)-specific nucleosomes and serve as an epigenetic mark for *CEN* identity and propagation. Cse4 is a critical determinant for the structure and function of the kinetochore and is required to ensure faithful chromosome segregation. The kinetochore protein Pat1 regulates the levels and spatial distribution of Cse4 at centromeres. Deletion of *PAT1* results in altered structure of *CEN* chromatin and chromosome segregation errors. In this study, we show that Pat1 protects *CEN*-associated Cse4 from ubiquitination in order to maintain proper structure and function of the kinetochore in budding yeast. *PAT1*-deletion strains exhibit increased ubiquitination of Cse4 and faster turnover of Cse4 at kinetochores. Psh1, a Cse4-specific E3-ubiquitin ligase, interacts with Pat1 in vivo and contributes to the increased ubiquitination of Cse4 in *pat1Δ* strains. Consistent with a role of Psh1 in ubiquitination of Cse4, transient induction of *PSH1* in a wild-type strain resulted in phenotypes similar to a *pat1Δ* strain, including a reduction in *CEN*-associated Cse4, increased Cse4 ubiquitination, defects in spatial distribution of Cse4 at kinetochores, and altered structure of *CEN* chromatin. Pat1 interacts with Scm3 and is required for its maintenance at kinetochores. In conclusion, our studies provide novel insights into mechanisms by which Pat1 affects the structure of *CEN* chromatin and protects Cse4 from Psh1-mediated ubiquitination for faithful chromosome segregation.

Monitoring Editor

Orna Cohen-Fix
National Institutes of Health

Received: Aug 29, 2014

Revised: Mar 11, 2015

Accepted: Mar 27, 2015

INTRODUCTION

The kinetochore is composed of centromeric (*CEN*) DNA, associated protein complexes, and a distinct chromatin structure (Bloom and Carbon, 1982) and is essential for faithful chromosome segregation in every eukaryotic system (Allshire and Karpen, 2008; Verdaasdonk and Bloom, 2011; Burrack and Berman, 2012; Choy et al., 2012; Maddox et al., 2012). The dissection of kinetochore structure and function of budding yeast has actively been pursued

since the discovery of centromeres in 1980 (Clarke and Carbon, 1980). About 71 kinetochore proteins have been identified (Lechner and Carbon, 1991; Pot et al., 2003; Crotti and Basrai, 2004; Cho et al., 2010; Gonen et al., 2012; Mishra et al., 2013); many of them are evolutionarily conserved, with orthologues found in fungi, flies, worms, and humans (Hartzog et al., 1996; Kitagawa and Hieter, 2001; Meraldi et al., 2006; Przewloka and Glover, 2009; Lampert and Westermann, 2011). Although *CEN* function is evolutionarily conserved, the *CEN* DNA sequence differs among organisms, ranging from the ~125 base pairs of unique DNA sequences in budding yeasts to several mega-base pairs of DNA composed of repeated sequences, species-specific satellite DNA arrays, or retrotransposon-derived sequences in other organisms (Clarke and Carbon, 1980; Allshire and Karpen, 2008; Verdaasdonk and Bloom, 2011; Burrack and Berman, 2012; Maddox et al., 2012). Despite such a variation in DNA sequence, *CEN* DNA in every eukaryotic organism examined so far is marked with specialized nucleosomes carrying an evolutionarily conserved histone H3 variant (Cse4 in budding yeast, Cnp1 in fission yeast, CID in fruit fly, HTR12 in *Arabidopsis*, and

This article was published online ahead of print in MBoc in Press (<http://www.molbiolcell.org/cgi/doi/10.1091/mbc.E14-08-1335>) on April 1, 2015.

Address correspondence to: Munira A. Basrai (basraim@mail.nih.gov).

Abbreviations used: *CEN*, centromere; CFP, cyan fluorescent protein; ChIP, chromatin immunoprecipitation; FACS, fluorescence-activated cell sorting; FRAP, fluorescence recovery after photobleaching; GFP, green fluorescent protein; qPCR, quantitative PCR.

© 2015 Mishra et al. This article is distributed by The American Society for Cell Biology under license from the author(s). Two months after publication it is available to the public under an Attribution–Noncommercial–Share Alike 3.0 Unported Creative Commons License (<http://creativecommons.org/licenses/by-nc-sa/3.0>).

“ASCB®,” “The American Society for Cell Biology®,” and “Molecular Biology of the Cell®” are registered trademarks of The American Society for Cell Biology.

CENP-A in humans; Allshire and Karpen, 2008; Verdaasdonk and Bloom, 2011; Burrack and Berman, 2012; Maddox et al., 2012). In budding yeast, ubiquitin-mediated proteolysis of Cse4 is important for kinetochore function and faithful chromosome segregation (Collins et al., 2004; Au et al., 2008, 2013; Deyter and Biggins, 2014). For example, an E3-ubiquitin ligase, Psh1, targets excess Cse4 for ubiquitination and proteolysis in order to prevent Cse4 mislocalization to non-CEN regions (Hewawasam et al., 2010, 2014; Ranjitkar et al., 2010). Because Psh1 also associates with CEN DNA, it is proposed that either the association of Cse4 with Scm3 and/or assembly of CEN chromatin exclude Psh1-mediated ubiquitination of CEN-associated Cse4 (Hewawasam et al., 2010).

We recently identified an evolutionarily conserved protein Pat1 (protein associated with topoisomerase II; *PATL1* in humans) as a structural component of budding yeast kinetochores (Mishra et al., 2013). Pat1 associates with CEN chromatin and regulates kinetochore structure to promote faithful chromosome segregation (Haase et al., 2013; Mishra et al., 2013). It is proposed that there are two pools of Cse4 molecules at the budding yeast kinetochores (Lawrimore et al., 2011; Haase et al., 2013). The core Cse4 molecules mediate attachment of kinetochores to microtubules, whereas the accessory (or peri-CEN) molecules may be required for the rapid assembly of Cse4 in case of its removal from the centromeres (Haase et al., 2013). Deletion of *PAT1* results in depletion of the peri-CEN Cse4 molecules (Haase et al., 2013; Scott and Bloom, 2014). However, the molecular mechanism by which Pat1 regulates Cse4 molecules at kinetochores remains unknown.

In this study, we report that Pat1 protects Cse4 from Psh1-mediated ubiquitination. In the absence of Pat1, we observed increased Cse4 ubiquitination regulated by the cell cycle and faster turnover of Cse4 at kinetochores. Transient induction of *PSH1* in a wild-type strain exhibits phenotypes similar to a *pat1Δ* strain, such as increased Cse4 ubiquitination, reduced Cse4 at kinetochores, and alterations in structural integrity of CEN chromatin. Pat1 interacts with Scm3 and regulates the centromeric levels of Scm3. Together our data uncover a novel Pat1-dependent mechanism for the maintenance of peri-CEN Cse4 molecules at kinetochores, which includes the protection of Cse4 from Psh1-mediated ubiquitination.

RESULTS

pat1Δ strains exhibit increased ubiquitination of Cse4

Pat1 is a structural component of the budding yeast kinetochore (Mishra et al., 2013), and deletion of *PAT1* exhibits reduction in CEN-associated Cse4 and depletion of peri-CEN Cse4 molecules (Haase et al., 2013). Ubiquitination of Cse4 by an E3-ubiquitin ligase, Psh1, regulates cellular levels of Cse4 (Hewawasam et al., 2010; Ranjitkar et al., 2010; Au et al., 2013). Because Psh1 associates with CEN DNA (Hewawasam et al., 2010), we reasoned that reduced levels of Cse4 at CEN DNA in *pat1Δ* strains (Haase et al., 2013) may be due to increased ubiquitination of Cse4. Hence we examined the ubiquitination state of endogenously expressed Cse4 in wild-type and *pat1Δ* strains. Controls included a strain expressing *cse4^{16KR}*, a mutant allele of Cse4 that cannot be ubiquitinated because all lysine residues are replaced with arginine (Ranjitkar et al., 2010; Au et al., 2013), and an untagged wild-type strain. Agarose beads with tandem ubiquitin-binding entities (Ub⁺) were used in an affinity assay (Hjerpe et al., 2009; Au et al., 2013) to pull down ubiquitin-associated proteins, and ubiquitination status of Cse4 was examined by Western blot analysis. Untagged wild-type and *cse4^{16KR}* strains do not show a laddering pattern for Cse4 (Figure 1A, lanes 3 and 4). A faster-migrating species is observed in the Ub⁺ pull down from all strains that were similar in size to the input band. Because

cse4^{16KR} cannot be ubiquitinated (Ranjitkar et al., 2010), this faster-migrating species likely represents unmodified forms of Cse4, which interact with ubiquitinated proteins bound to Ub⁺ agarose. Similar observations were made previously in Ub⁺ affinity agarose experiments with wild-type Cse4 and *cse4^{16KR}* (Au et al., 2013; Hewawasam et al., 2014). In a logarithmically growing culture, higher levels of ubiquitinated Cse4 were observed in a *pat1Δ* strain, as evident from the laddering pattern when compared with the wild-type strain (Figure 1A, lanes 7 and 8 and input control lanes 5 and 6). To examine whether Cse4 ubiquitination is affected by the cell cycle stage, we assayed ubiquitination of Cse4 in wild-type and *pat1Δ* strains that were synchronized in G1 (α -factor treatment), S (hydroxyurea treatment), and G2/M (nocodazole treatment) stages of the cell cycle. Hydroxyurea blocks the synthesis of deoxyribonucleotides, inducing a DNA replication-dependent checkpoint in S phase (Weinert et al., 1994), whereas nocodazole inhibits polymerization of microtubules, leading to a cell cycle arrest in mitosis (Jacobs et al., 1988). The cell cycle synchronization was verified by fluorescence-activated cell sorting (FACS) analysis (Supplemental Figure S1A). In wild-type cells, the ubiquitination of Cse4 was much higher in mitotic (G2/M) cells (Figure 1A, lane 19 and input control lane 17), and was barely detectable in G1 and S phase-arrested cells (Figure 1A, lanes 11 and 15 and input control lanes 9 and 13). In a *pat1Δ* strain, maximum Cse4 ubiquitination was also observed in mitotic (G2/M) cells (Figure 1A, lane 20 and input control lane 18), however, it was consistently higher than the wild-type strain in all cell cycle stages examined (Figure 1A, lanes 12, 16, and 20, and input control lanes 10, 14, and 18). Control experiments performed with a wild-type strain with agarose beads without Ub-binding activity (Ub⁻) do not exhibit a laddering pattern for Cse4 (Figure 1A, lane 21). Next we quantified the fraction of ubiquitinated Cse4 and normalized this to the total Cse4 levels (input) in each stage of the cell cycle as described previously (Au et al., 2013). The enrichment of ubiquitinated Cse4 was significantly higher (two-fold to threefold) in mitotic (G2/M) cells than in the G1 or S phase cells (Figure 1B). The increased ubiquitination of Cse4 in mitosis was verified by assaying cells synchronized in G1 (α -factor treatment) and released into pheromone-free medium (Supplemental Figure S2, A–D). Consistent with the increased ubiquitination of Cse4 in nocodazole-treated cells (Figure 1A), higher levels of ubiquitinated Cse4 were observed in cells undergoing mitosis (Supplemental Figure S2, A–D). To determine whether only ubiquitination of Cse4 is increased in *pat1Δ* strains or the overall ubiquitination activity is up-regulated, we examined the ubiquitination of histone H2B in wild-type and *pat1Δ* strains. The levels of histone H2B ubiquitination were largely similar between wild-type and *pat1Δ* strains, suggesting that the increased ubiquitination of Cse4 in a *pat1Δ* strain is specific to Cse4 (Supplemental Figure S2E).

To confirm further and validate the use of Ub⁺ agarose for ubiquitination status of Cse4, we immunoprecipitated endogenously expressed Myc-tagged Cse4 and examined the ubiquitination status of Cse4 by Western blot analysis using anti-ubiquitin and anti-Myc antibodies. Consistent with results from Ub⁺ experiments (Figure 1A), higher levels of Cse4 ubiquitination were observed in a *pat1Δ* strain than with the wild-type strain (Figure 1C). Control experiments with an untagged strain do not exhibit a laddering pattern for Cse4 (Figure 1C).

Chromatin immunoprecipitation (ChIP) experiments followed by quantitative PCR (qPCR) were done to examine whether the increased ubiquitination of Cse4 in *pat1Δ* strains may be due to higher levels of Psh1 at CEN. CEN levels of Psh1 in a logarithmically growing culture were not significantly different between the wild-type

(1.46% of input at *CEN1* and 1.38% at *CEN3*) and *pat1Δ* (1.92% at *CEN1* and 2.03% at *CEN3*) strains, although slightly higher levels were observed in *pat1Δ* strains (Figure 1D). To examine whether *CEN* association of Psh1 is cell cycle regulated, we did ChIP experiments using cells synchronized in G1 with α -factor, in S phase with hydroxyurea, or in G2/M with nocodazole treatment. Cell cycle synchronization was confirmed by FACS analysis (Supplemental Figure S1B). No significant enrichment of Psh1 was detected at either *CEN* or non-*CEN ACT1* regions in ChIP-qPCR experiments with an untagged strain (Supplemental Figure S3). *CEN* levels of Psh1 were not significantly different between wild-type and *pat1Δ* strains in G1 and S phase of the cell cycle (Figure 1D). However, in G2/M cells, *CEN* levels of Psh1 were significantly higher in the *pat1Δ* strain (2.31% at *CEN1* and 2.33% at *CEN3*) than the wild type (1.54% at *CEN1* and 1.69% at *CEN3*; $p < 0.05$; Figure 1D). No significant enrichment of Psh1 was observed at *ACT1* locus used as a control (Figure 1D). Protein expression level of Psh1 was similar between the wild-type and *pat1Δ* strains (Figure 1E).

Centromeric Cse4 exchanges rapidly in *pat1Δ* strains

Increased ubiquitination of Cse4 (Figure 1A) and depletion of peri-*CEN* Cse4 molecules in a *pat1Δ* strain (Haase et al., 2013) suggest that Pat1 may protect *CEN*-bound Cse4 from ubiquitination and make it more stable at the kinetochore. Hence we examined whether a deletion of *PAT1* results in a faster exchange of Cse4-GFP at metaphase kinetochores by using a fluorescence recovery after photobleaching (FRAP) assay (Pearson et al., 2004). The Cse4-GFP strain does not exhibit growth defects at 25 and 38°C, suggesting that GFP tagging of Cse4 does not affect its function (Figure 2A). Cse4-GFP-labeled centromeres were photobleached, and FRAP (pre and post) was followed at 1-min intervals for 10 min. The average fluorescence recovery of Cse4-GFP after photobleaching in the wild-type strain was low at $\sim 13\% \pm 3$ (mean \pm SE, $n = 6$, after 5 min), indicating that Cse4 is a stable component of the kinetochore and that centromeres remained positioned within their respective spindle half after metaphase congression (Figure 2B). The low level of Cse4-GFP fluorescence recovery as observed here for the wild-type strain has been reported previously (Pearson et al., 2004; Lawrimore et al., 2011). Consistent with our hypothesis, the average Cse4-GFP fluorescence recovery in the *pat1Δ* strain was $23\% \pm 5$ (mean \pm SE, $n = 13$, after 5 min; Figure 2, B–D, and Supplemental Figure S4), which is significantly faster than that for the wild-type strain ($p < 0.05$). Taken together, these observations support the conclusion that Pat1 is required for stable maintenance of Cse4 at the kinetochores and protects it from ubiquitination.

Psh1 contributes to the increased ubiquitination of Cse4 in a *pat1Δ* strain

The increased ubiquitination of Cse4 and higher levels of *CEN*-bound Psh1 in *pat1Δ* strains (Figure 1, A and C) during mitosis prompted us to investigate whether Psh1 contributes to the increased ubiquitination of Cse4 in the *pat1Δ* strain. We created a *pat1Δ psh1Δ* strain and assayed the ubiquitination of Cse4 in this strain and compared it to that of wild-type, *pat1Δ*, and *psh1Δ* strains. No laddering pattern for Cse4 was observed in control experiments performed with a wild-type strain using agarose beads without Ub-binding activity (Ub⁻; Figure 3A, lane 9). As observed previously (Figure 1A), the ubiquitination of Cse4 was much higher in the *pat1Δ* strain (Figure 3A, lane 6 and input control lane 2) than the wild-type strain (Figure 3A, lane 5 and input control lane 1). Consistent with previous reports, Cse4 ubiquitination was greatly diminished in the *psh1Δ* strain (Figure 3A, lane 7 and input control lane 3). The

increased ubiquitination of Cse4 observed in *pat1Δ* strains was also diminished in the *pat1Δ psh1Δ* strain (Figure 3A, lane 8 and input control lane 4).

Next we performed ChIP-qPCR to examine the levels of Cse4 at kinetochores in these strains. In agreement with previous observations (Haase et al., 2013), the levels of Cse4 at *CENs* (*CEN1*, *CEN3*, and *CEN5*) were reduced in *pat1Δ* strains (Figure 3B). Consistent with the ubiquitination state of Cse4 (Figure 3A), the levels of Cse4 at kinetochores were higher in the *pat1Δ psh1Δ* strain than in the *pat1Δ* strain (Figure 3B). To examine whether Pat1 interacts with Psh1 in vivo, we performed immunoprecipitation experiments using a strain that expressed both Flag-tagged Pat1 and TAP-tagged Psh1 from their endogenous promoters. Our results showed an interaction between Pat1 and Psh1 (Figure 3C). No interactions were observed in control experiments using a wild-type strain carrying only TAP-tagged Psh1 (Figure 3C). Taken together, these observations show that Psh1 contributes to increased ubiquitination of Cse4 in a *pat1Δ* strain.

Previous studies showed an in vivo interaction between Psh1 and Cse4 (Hewawasam et al., 2010; Ranjitkar et al., 2010). We did immunoprecipitation experiments to determine whether the increased ubiquitination of Cse4 in *pat1Δ* strains is due to altered interaction of Psh1 and Cse4 in these strains. Experiments were done with wild-type and *pat1Δ* strains expressing TAP-tagged Psh1 and HA-tagged Cse4 from their endogenous promoters. The interaction of Psh1 and Cse4 is not significantly different in the *pat1Δ* strains compared to the wild-type strain (Figure 3D). No signals were observed in control experiments using a wild-type strain carrying only TAP-tagged Psh1 (Figure 3D).

Induction of *PSH1* results in increased Cse4 ubiquitination, reduction in centromere-associated Cse4, and altered spatial distribution of Cse4 at kinetochores

Our results show that Psh1 contributes to increased ubiquitination of Cse4 in a *pat1Δ* strain. Hence we examined whether transient induction of *PSH1* exhibits phenotypes similar to those observed in a *pat1Δ* strain. Because constitutive overexpression of *PSH1* causes loss of viability in wild-type and *pat1Δ* strains (Supplemental Figure S5), all experiments were done with a *GALPSH1* strain grown for 6 h in galactose medium (Figure 4, A and B). In agreement with our hypothesis, transient induction of *PSH1* showed increased Cse4 ubiquitination in a wild-type strain compared with the vector control (Figure 4B, lanes 6 and 8). Higher levels of ubiquitinated Cse4 were observed in a *pat1Δ* strain; however, no major differences in Cse4 ubiquitination with and without induction of *PSH1* were observed in a *pat1Δ* strain (Figure 4B, lanes 7 and 9). Control experiments performed using chromatin extracts from the wild-type strain with agarose beads without Ub-binding activity (Ub⁻) exhibited no laddering pattern for Cse4 (Figure 4B, lane 5). Consistent with the role of Psh1 in Cse4 proteolysis (Hewawasam et al., 2010; Ranjitkar et al., 2010), transient induction of *PSH1* in a wild-type strain caused faster degradation of Cse4 (approximately sixfold to sevenfold) than the vector control (Figure 4, C and D).

ChIP experiments were used to determine whether increased ubiquitination of Cse4 contributes to lower levels of Cse4 at *CEN* in *GALPSH1* strains. ChIP-qPCR revealed that the level of *CEN*-associated Cse4 was reduced significantly in wild-type and *pat1Δ* strains with *GALPSH1* when compared to the levels observed in a wild-type strain with vector alone (Figure 5A). Of note, the transient induction of *PSH1* in a wild-type strain exhibits *CEN*-associated Cse4 levels similar to those observed in a *pat1Δ* strain (Figure 5A). No significant enrichment of Cse4 was observed at the non-*CEN HML* locus (Figure 5A).

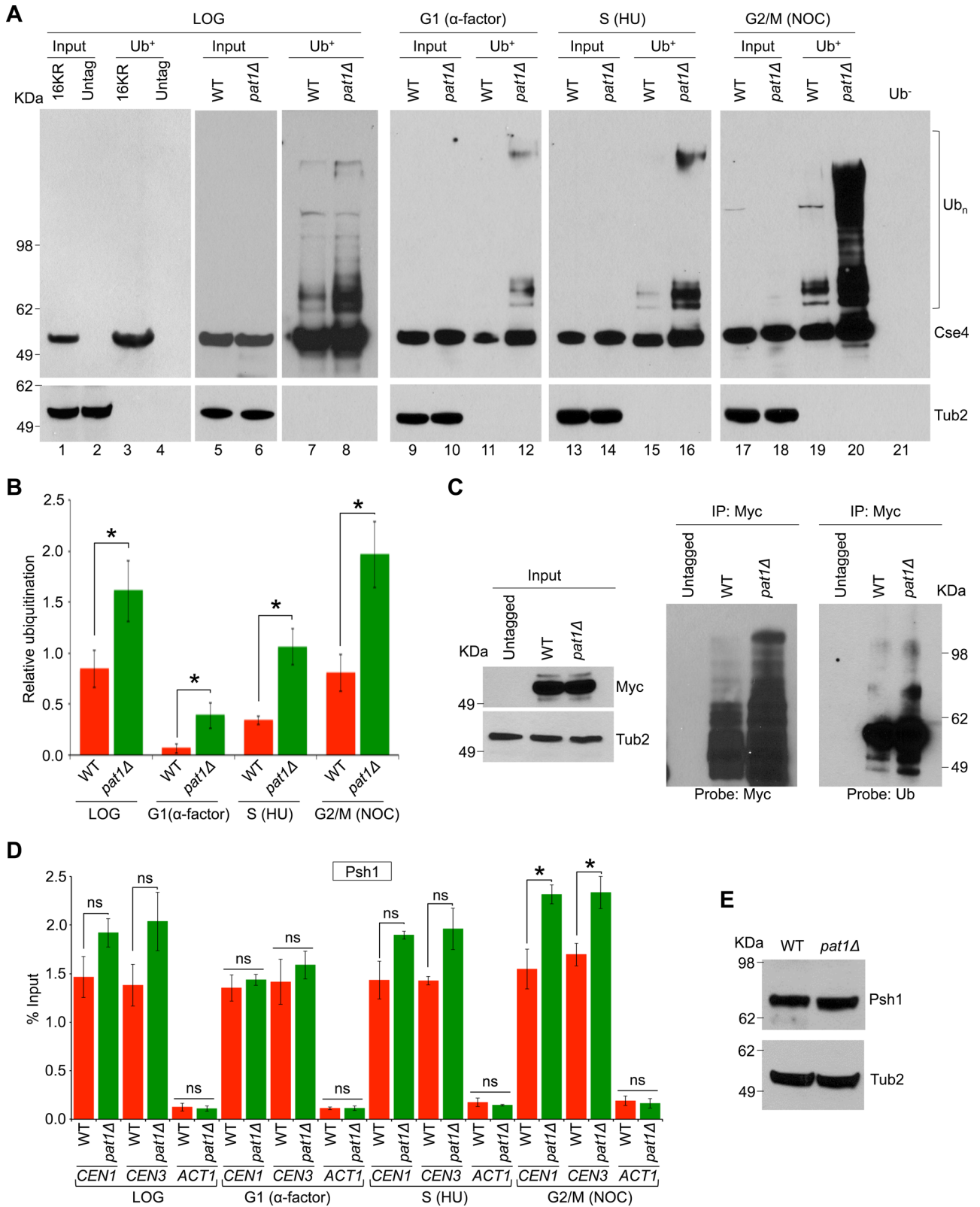


FIGURE 1: Cse4 ubiquitination is cell cycle dependent and is increased in *pat1* Δ strains. (A) Cell cycle-dependent ubiquitination of Cse4, which is increased in a *pat1* Δ strain. Western blotting showing the levels of Cse4 ubiquitination (Ub_n) in wild-type (WT, YMB6398) and *pat1* Δ (YMB8422) strains in cells grown to different stages of the cell cycle: logarithmic phase (LOG), G1 cells synchronized with α -factor, S phase cells synchronized with (HU), and G2/M cells synchronized with nocodazole (NOC). Wild-type strain with mutant *cse4*^{16KR} in which all lysine residues are changed to arginine (16KR; Au *et al.*, 2013) and an untagged strain (untag; YPH499) were used as control in ubiquitin pull-down experiments. Eluted proteins were analyzed by Western blotting with α -Myc (Cse4) or α -Tub2 (served as a loading control) antibodies. Molecular weight markers for protein size in kilodaltons. (B) Quantification of relative ubiquitination

We previously showed that reduced levels of *CEN*-bound Cse4 contribute to its altered spatial distribution in *pat1Δ* strains (Haase et al., 2013). Given the similarity of phenotypes of *pat1Δ* with the transient induction of *PSH1*, we reasoned that spatial distribution of Cse4 at metaphase kinetochores could be altered in *GALPSH1* strains. Our results supported this hypothesis, as the spot width of Cse4, which spans 678 nm, was decreased to 513 nm upon transient induction of *PSH1* in a wild-type strain (Figure 5B). Consistent with our previous results (Haase et al., 2013), a decrease of Cse4 spot width to 595 nm was observed in a *pat1Δ* strain. The spatial distribution of Cse4 remained unaltered upon transient induction of *PSH1* in a *pat1Δ* strain (Figure 5B). Induction of *PSH1* specifically affects the distribution of Cse4, as the distribution of another kinetochore protein, Ndc80, was not altered in a *GALPSH1* strain (Supplemental Figure S6) or a *pat1Δ* strain (Haase et al., 2013).

Induction of *PSH1* results in structural changes of *CEN* chromatin and kinetochores

The reduced levels of *CEN*-associated Cse4 led us to examine whether transient induction of *PSH1* causes defects in the structural integrity of *CEN* chromatin similar to that observed in a *pat1Δ* strain, by using *Dral* accessibility assay (Saunders et al., 1990; Meluh et al., 1998; Myhre and Bloom, 2003; Crotti and Basrai, 2004; Yu et al., 2011; Mishra et al., 2013). Induction of *PSH1* increased *Dral* accessibility of *CEN3* chromatin in a wild-type strain (sixfold to eightfold) compared to the strain with vector alone (Figure 6). In agreement with previous results (Mishra et al., 2013), increased *Dral* accessibility of *CEN3* chromatin was observed in the *pat1Δ* strain with vector alone (Figure 6). There was a slightly higher *Dral* accessibility of *CEN3* in the *pat1Δ+GALPSH1* strain, although this was not statistically significant. Deletion of *PAT1* or transient overexpression of *PSH1* did not affect the structure at non-*CEN* regions such as *ADP1* (*H3* chromatin; Figure 6).

Next we examined whether induction of *PSH1* alters the two-dimensional distribution of Cse4 at the kinetochores similar to that observed in a *pat1Δ* strain (Haase et al., 2013). The distance of Cse4 from the spindle pole body and the spread of Cse4 perpendicular to the spindle pole body were measured. Cse4 distribution in both the wild-type and *pat1Δ* strains was within 5 nm relative to the spindle pole body (distance from spindle pole: wild type, 286 ± 120 nm; *pat1Δ*, 281 ± 74 nm). However, the spread of Cse4 perpendicular to the spindle (width across spindle) was reduced about twofold in *pat1Δ* strains (wild type, 181 ± 155 nm; *pat1Δ*, 108 ± 102 nm; Haase et al., 2013). Cse4 distribution in the wild-type strain without *PSH1* overexpression was similar to previous observations (distance from spindle pole, 285 ± 122 nm; width across spindle,

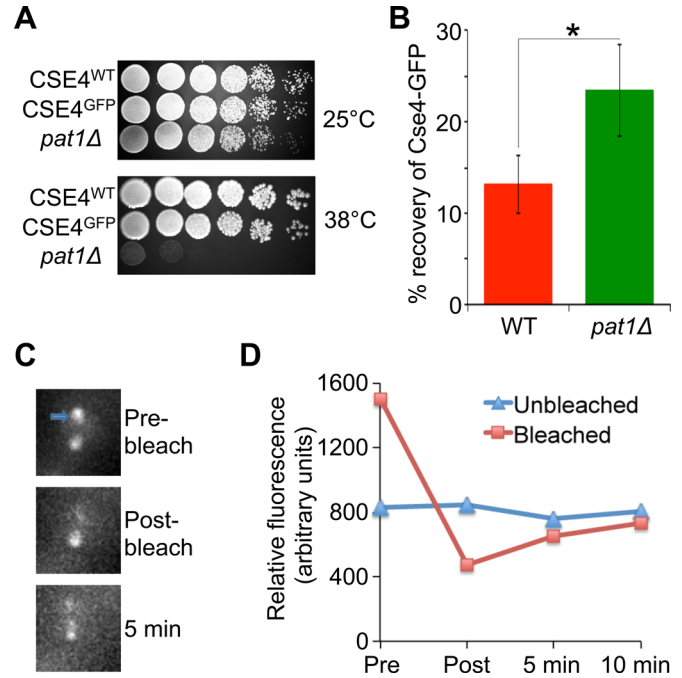


FIGURE 2: Cse4 exchange at kinetochores is faster in *pat1Δ* strains. (A) Cse4-GFP strains do not exhibit growth defects or temperature sensitivity to growth phenotypes. Serial dilutions (fivefold) of WT (KBY8116), Cse4-GFP (KBY2012), and *pat1Δ* (YMB8936) strains grown on YPD at 25 and 38°C. (B) Average Cse4-GFP fluorescence recovery for WT (KBY2012) and *pat1Δ* (KBY8166) strains 5 min postbleaching ± SE. **p* < 0.05, Student's *t* test. (C) Representative images showing photobleaching and recovery of Cse4-GFP fluorescence in a *pat1Δ* strain. Cse4-GFP-labeled centromeres were photobleached during metaphase. One of the two kinetochore clusters was bleached (blue arrow). Fluorescence recovery observed after 5 min of photobleaching. (D) Fluorescence recovery of the bleached spot in a *pat1Δ* strain from representative image shown in C.

183 ± 155 nm; *n* = 208; Figure 7A; Haase et al., 2013). However, the wild-type strain with transiently induced *PSH1* levels exhibited a change in the two-dimensional structure of Cse4 similar to that observed for a *pat1Δ* strain. The distance of Cse4 from the spindle pole was 242 ± 111 nm, whereas the spread of Cse4 perpendicular to the spindle (width across spindle) was reduced to 102 ± 95 nm (*n* = 204; Figure 7B). Transient induction of *PSH1* in a *pat1Δ* strain did not further exacerbate the two-dimensional structure of Cse4 (Haase et al., 2013).

of Cse4 in different cell cycle stages. Ratio of ubiquitinated Cse4 (bracket in A) to the total Cse4 levels (input) in WT and *pat1Δ* strains was calculated. The histogram represents the average of three biological replicates with SE. **p* < 0.05, Student's *t* test. Statistically significant differences were observed between G1 and S or G2/M phases of the cell cycle in WT (*p* values: G1 vs. S, 0.004; G1 vs. G2/M, 0.008; S vs. G2/M, 0.034) and *pat1Δ* (*p* values: G1 vs. S, 0.019; G1 vs. G2/M, 0.005; S vs. G2/M, 0.037) strains. (C) Ubiquitination of Cse4 is increased in a *pat1Δ* strain. Western blotting showing the levels of Cse4 ubiquitination in wild-type (WT, YMB6398), *pat1Δ* (YMB8422), and untagged control (YPH499) strains grown to logarithmic phase of growth. Endogenously expressed Cse4-Myc was immunoprecipitated. Eluted proteins were analyzed by Western blotting with α-Myc (Cse4), α-Ub, or α-Tub2 (served as a loading control) antibodies. Molecular weight markers for protein size in kilodaltons. (D) Association of Psh1 with *CEN* chromatin through the cell cycle. ChIP-qPCR showing the levels of Psh1 in WT (YMB8126) and *pat1Δ* (YMB9096) strains at *CEN* (*CEN1*, *CEN3*) and non-*CEN* (*ACT1*) regions. Enrichment was determined by qPCR and is shown as percentage input. Average from three biological experiments ± SE. **p* < 0.05; ns, statistically not significant, Student's *t* test. (E) Western blotting using α-TAP antibodies revealed that protein levels of Psh1 are not different between WT (YMB8126) and *pat1Δ* (YMB9096) strains. Molecular weight markers for protein size in kilodaltons.

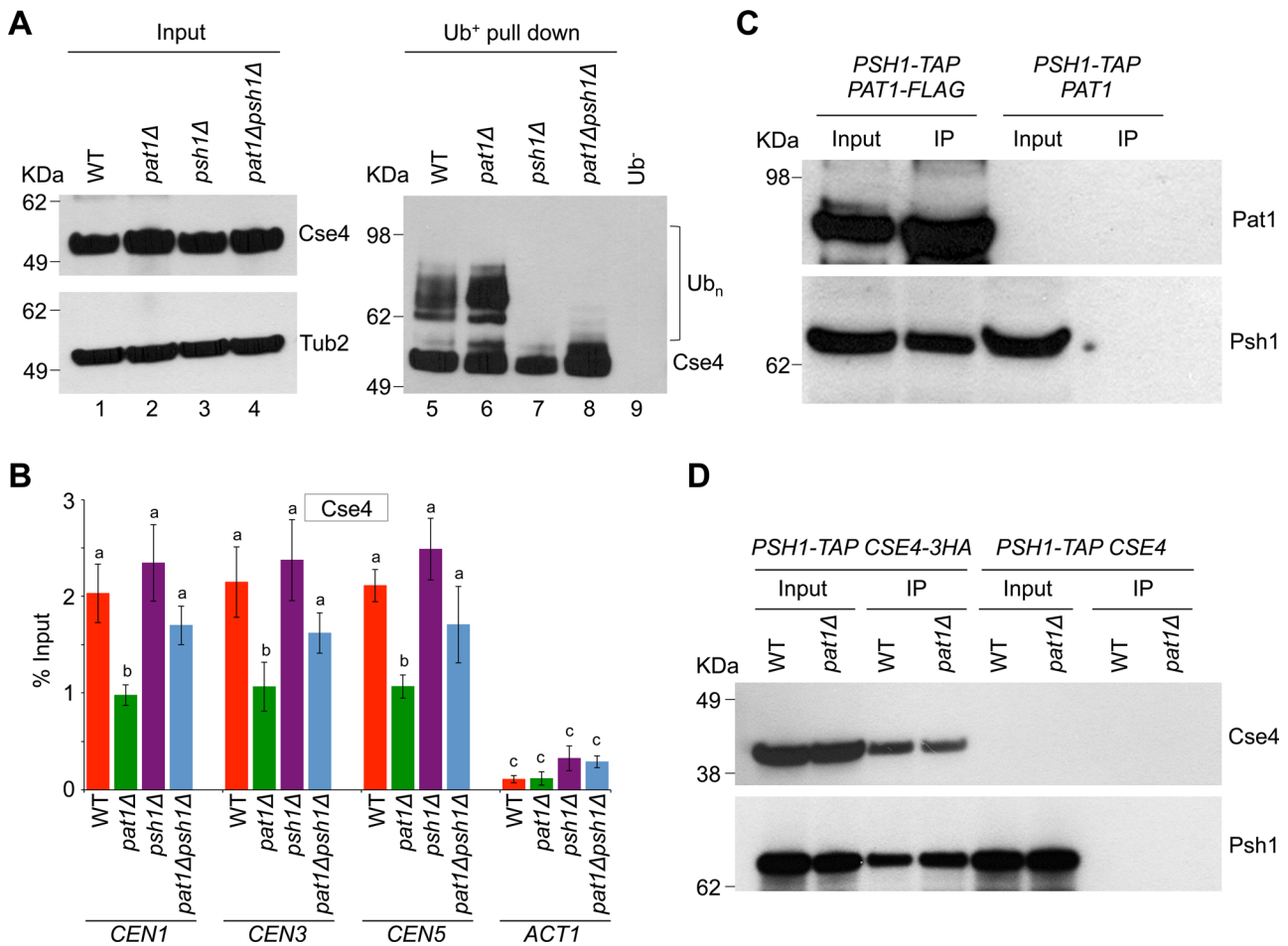


FIGURE 3: Psh1 contributes to the ubiquitination of Cse4 in a *pat1Δ* strain. (A) Deletion of *PSH1* reduces the levels of Cse4 ubiquitination in a *pat1Δ* strain. Western blotting showing the levels of Cse4 ubiquitination (Ub_n) in logarithmic growing cultures of WT (YMB6398), *pat1Δ* (YMB8422), *psh1Δ* (YMB9311), and *pat1Δpsh1Δ* (YMB9312) strains. Antibodies used were α -Myc (Cse4) or α -Tub2 (served as a loading control). Molecular weight markers for protein size in kilodaltons. (B) Deletion of *PSH1* results in higher levels of Cse4 at kinetochores in the *pat1Δ psh1Δ* strain. WT (YMB6398), *pat1Δ* (YMB8422), *psh1Δ* (YMB9311), and *pat1Δpsh1Δ* (YMB9312) strains were grown to logarithmic phase of growth in YPD at 30°C, and ChIP for Cse4 was performed. The enrichment levels of Cse4 at *CEN* (*CEN1*, *CEN3*, *CEN5*) and non-*CEN* (*ACT1*) regions are presented. Enrichment was determined by qPCR and is shown as percentage input. Average from three biological experiments \pm SE. Values sharing the same letter are not significantly different at a 5% level based on analysis of variance ($p > 0.05$). (C) Pat1 interacts in vivo with Psh1. Immunoprecipitation experiments were done using agarose beads conjugated with α -Flag antibodies using cell extracts from strain YMB9280 expressing Flag-tagged Pat1 and TAP-tagged Psh1 (*PSH1-TAP PAT1-FLAG*) and a control strain YMB8126 expressing TAP-tagged Psh1 (*PSH1-TAP PAT1*) from their native promoters. Strains were grown in YPD at 30°C. Eluted proteins were analyzed by Western blotting with α -Flag (Pat1) and α -TAP (Psh1) antibodies. Molecular weight markers for protein size in kilodaltons. (D) Deletion of *PAT1* does not significantly affect the in vivo interaction between Psh1 and Cse4. Immunoprecipitation experiments were performed using agarose beads conjugated with α -HA antibodies using cell extracts from WT (YMB9281) and *pat1Δ* (YMB9282) strains expressing TAP-tagged Psh1 and HA-tagged Cse4 (*PSH1-TAP CSE4-3HA*) from their native promoters. For control experiments, WT (YMB8126) and *pat1Δ* (YMB9096) strains expressing TAP-tagged Psh1 (*PSH1-TAP CSE4*) from their native promoters were used. Strains were grown in YPD at 30°C. Eluted proteins were analyzed by Western blotting with α -HA (Cse4) and α -TAP (Psh1) antibodies. Protein signals were quantified using ImageJ software (Schneider et al., 2012). Molecular weight markers for protein size in kilodaltons.

Pat1 interacts with Scm3 and *pat1Δ* strains showed reduced levels of centromeric Scm3

The kinetochore protein Scm3 is a Cse4-specific assembly factor and protects centromeric Cse4 from Psh1-mediated ubiquitination (Hewawasam et al., 2010). Because reduced levels of peri-*CEN* Cse4 contribute to its altered spatial distribution in *pat1Δ* strains (Haase et al., 2013), we examined whether Pat1 interacts with Scm3 in vivo and affects the levels of centromeric Scm3. We constructed a

strain that expressed HA-tagged Pat1, Flag-tagged Scm3, and Myc-tagged Cse4 from their endogenous promoters. No signals were observed in a control experiment using an untagged Pat1 strain (Figure 8A). As previously reported, we observed an interaction between Scm3 and Cse4 (Camahort et al., 2007; Mizuguchi et al., 2007; Stoler et al., 2007; Mishra et al., 2011). Immunoprecipitation results showed that Pat1 interacts with Scm3 and Cse4 but not with histone H3 in vivo.

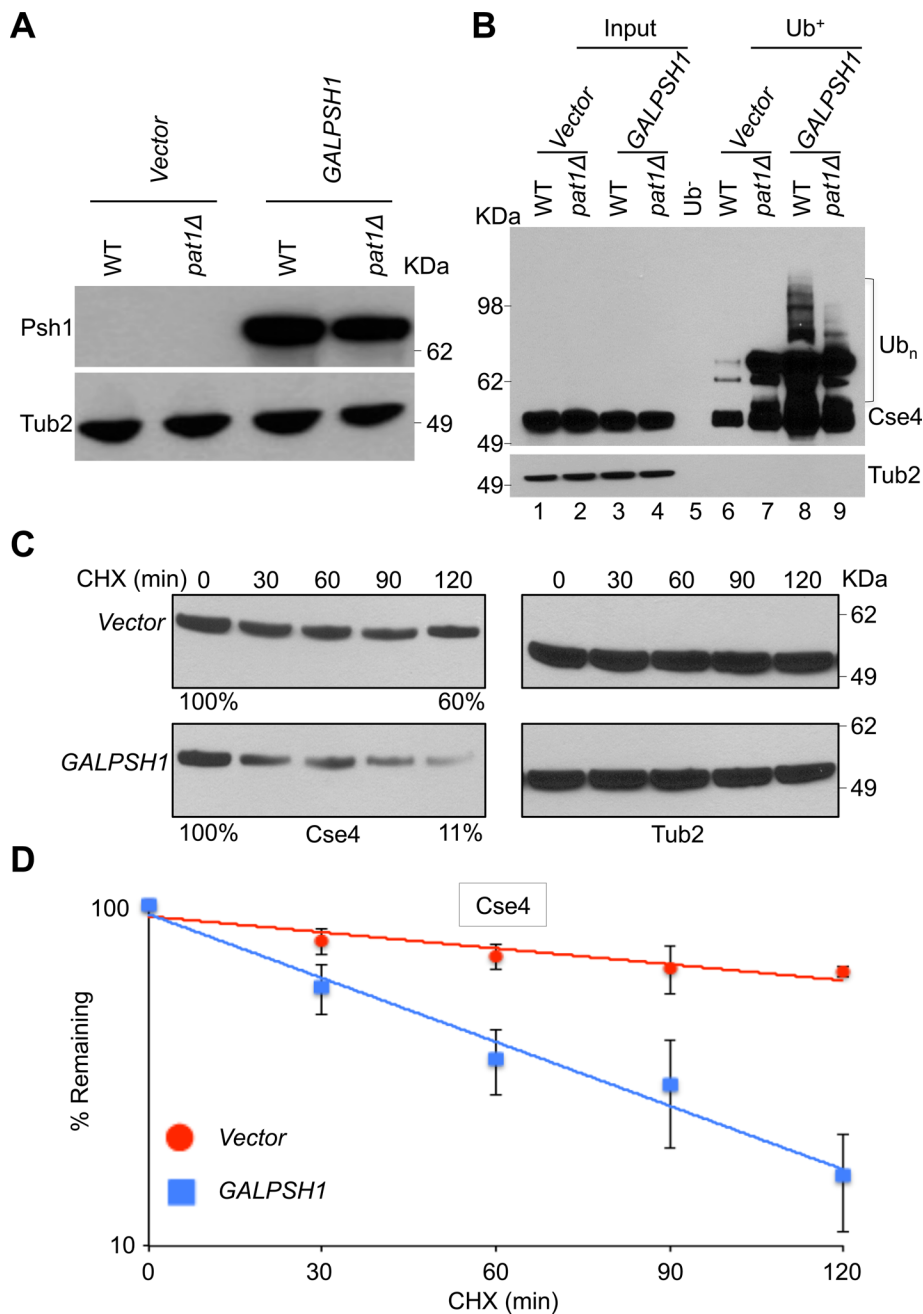


FIGURE 4: Induction of Psh1 causes increased ubiquitination and increased proteolysis of Cse4. (A) Western blot analysis was done using whole-cell protein extracts prepared from WT (YMB6398) and *pat1Δ* (YMB8948) strains transformed with vector (pRS426 GAL1) or *GALPSH1HA* (pMB1628). Strains were grown to logarithmic phase of growth in synthetic medium, and gene expression was induced in the presence of galactose plus raffinose (2% each) at 30°C for 6 h. Blots were probed with α -HA for expression of *GALPSH1HA* and α -Tub2 (served as a loading control) antibodies. Molecular weight markers for protein size in kilodaltons. (B) Transient induction of *PSH1* increases Cse4 ubiquitination. Western blotting showing the levels of Cse4 ubiquitination in WT (YMB6398) and *pat1Δ* (YMB8948) strains transformed with vector (pRS426 GAL1) or *GALPSH1HA* (pMB1628). Strains were grown to logarithmic phase of growth in synthetic medium, and gene expression was induced in the presence of galactose plus raffinose (2% each) at 30°C for 6 h. Ubiquitin pull down was performed as described in *Materials and Methods*. Eluted proteins were analyzed by Western blotting with α -Myc (Cse4) or α -Tub2 (served as a loading control) antibodies. Molecular weight markers for protein size in kilodaltons. (C) Transient induction of *PSH1* causes increased proteolysis of Cse4. WT (YMB6398) strains transformed with vector (pRS426 GAL1) or *GALPSH1HA* (pMB1628) were grown to logarithmic phase of growth in synthetic medium, and gene expression was induced in the presence of galactose plus raffinose (2% each) at 30°C for 6 h. Cycloheximide (100 μ g/ml) was added to the cultures, and samples were collected at indicated time intervals. Protein extracts were prepared

ChIP-qPCR experiments showed that the level of CEN-associated Scm3 was reduced significantly in *pat1Δ* (0.71% of input at *CEN1*, 0.70% at *CEN3*, and 0.56% at *CEN5*) compared with the levels observed in a wild-type strain (1.97% at *CEN1*, 1.80% at *CEN3*, and 1.56% at *CEN5*; Figure 8B). No significant enrichment of Scm3 was detected at the non-CEN *HML* locus (Figure 8B). Western blotting revealed that the reduction in CEN-associated Scm3 in the *pat1Δ* strain was not due to reduction in the protein levels of Scm3 (Figure 8C). The interaction of Pat1 with Scm3 and the reduced levels of centromeric Scm3 suggest that Pat1, together with Scm3, plays a critical role in protecting centromeric Cse4 from Psh1-mediated ubiquitination.

DISCUSSION

Evolutionarily conserved histone H3 variant Cse4 and its homologues are essential for chromosome segregation (Allshire and Karpen, 2008; Verdaasdonk and Bloom, 2011; Burrack and Berman, 2012; Maddox *et al.*, 2012). In budding yeast, two pools of Cse4 molecules have been identified at kinetochores (Lawrimore *et al.*, 2011; Haase *et al.*, 2013). The complex with core Cse4 molecules interacts with kinetochore microtubules, and the accessory Cse4 molecules that reside at the peri-CEN region may be required for rapid assembly of Cse4 upon eviction from centromeres (Haase *et al.*, 2013). Peri-CEN Cse4 pools are reduced in a *pat1Δ* strain, which exhibits defects in chromosome segregation and altered structure of CEN chromatin (Haase *et al.*, 2013; Mishra *et al.*, 2013; Scott and Bloom, 2014). Here we show that Pat1 interacts with Scm3 and E3-ubiquitin ligase Psh1 to maintain peri-CEN Cse4 at kinetochores by protecting it from Psh1-mediated ubiquitination. These conclusions are based on results showing that *pat1Δ* strains exhibit 1) an increase in Cse4 ubiquitination, 2) a faster turnover of Cse4 at kinetochores, 3) reduced Cse4 ubiquitination when combined with *psh1Δ*, and 4) reduced levels of centromeric Scm3. Furthermore, transient induction of *PSH1* in a wild-type strain exhibits phenotypes similar

and analyzed by Western blotting with α -Myc (Cse4) or α -Tub2 (served as a loading control) antibody. Molecular weight markers for protein size in kilodaltons. (D) Rate of Cse4 degradation is faster in a WT strain with transient induction of *PSH1*. Signal intensities from Western blots shown in C were quantified and statistically analyzed as described previously (Au *et al.*, 2008). Average from three biological experiments \pm SE.

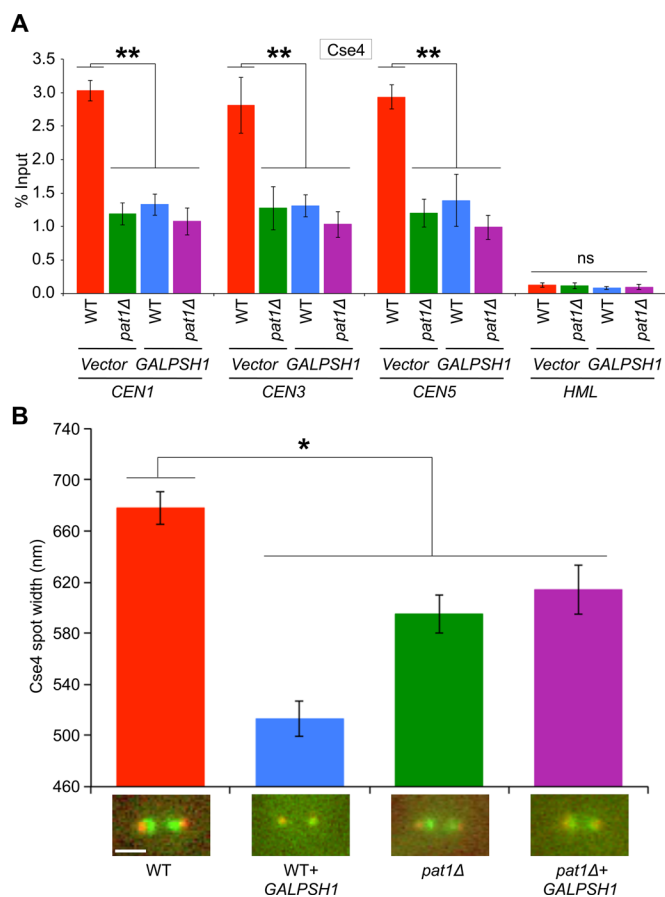


FIGURE 5: Induction of Psh1 causes reduction in CEN levels of Cse4, and its spatial distribution is altered at the kinetochores. (A) Transient induction of *PSH1* causes reduction in CEN levels of Cse4. WT (YMB6398) and *pat1Δ* (YMB8948) strains transformed with vector (pRS426 *GAL1*) or *GALPSH1HA* (pMB1628) were grown to logarithmic phase of growth in synthetic medium, and gene expression was induced in the presence of galactose plus raffinose (2% each) at 30°C for 6 h. ChIP for Cse4 was performed. The enrichment levels of Cse4 at CEN (*CEN1*, *CEN3*, *CEN5*) and non-CEN (*HML*) regions are presented. Enrichment was determined by qPCR and is shown as percentage input. Average from three biological experiments \pm SE. $**p < 0.01$, ns, statistically not significant, Student's *t* test. (B) Transient induction of *PSH1* causes alterations in the appearance of Cse4 at kinetochores. The height of the cluster of Cse4-GFP at kinetochores was determined from line scans (perpendicular to the spindle axis) through the protein cluster as previously described (Haase *et al.*, 2013). The height was determined from the full-width, full-maximum of the Gaussian distribution. The average spot width of Cse4-GFP foci is shown in WT (KBY2012) and *pat1Δ* (KBY8166) strains overexpressing *PSH1* (*GALPSH1HA*, pMB1628) for 6 h. Sample sizes range from 11 to 15 cells for each condition, and representative images from each condition are shown. $*p < 0.05$, Student's *t* test.

to a *pat1Δ* strain, such as increased Cse4 ubiquitination, reduction in CEN-associated Cse4, altered structure of CEN chromatin, and distribution of Cse4 at the kinetochores.

Our results show that Pat1 protects CEN-associated Cse4 pools from Psh1-mediated ubiquitination. A higher enrichment of ubiquitinated Cse4 was observed in a *pat1Δ* strain, particularly in G2/M cells, which correlated with increased levels of CEN-associated Psh1. Consistent with this hypothesis, Cse4 molecules from

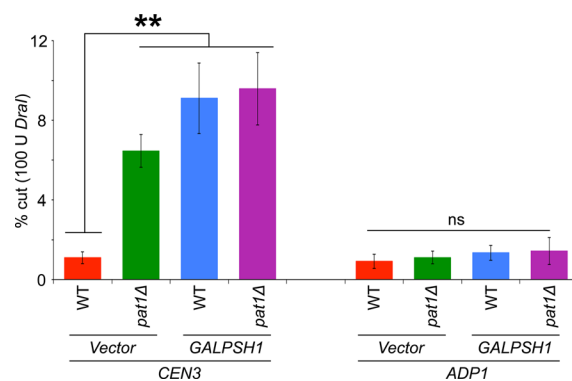


FIGURE 6: Induction of Psh1 causes structural alterations in CEN chromatin. Transient induction of *PSH1* increases the accessibility of *Dral* to CEN chromatin. WT (YMB6398) and *pat1Δ* (YMB8948) strains transformed with vector (pRS426 *GAL1*) or *GALPSH1HA* (pMB1628) were grown to logarithmic phase of growth in synthetic medium, and gene expression was induced in the presence of galactose plus raffinose (2% each) at 30°C for 6 h. Nuclei were prepared and treated with *Dral* restriction enzyme to measure enzymatic accessibility as described previously (Mishra *et al.*, 2013). *Dral* accessibility of CEN chromatin (*CEN3*) is significantly increased upon overexpression of *PSH1* in WT and *pat1Δ* strains but had no significant affect at H3-chromatin (*ADP1*). Average from three biological experiments \pm SE. $**p < 0.01$, ns, statistically not significant, Student's *t* test.

peri-CEN chromatin were depleted in a *pat1Δ* strain (Haase *et al.*, 2013). We propose that the macromolecular kinetochore complex protects the core Cse4 molecules and renders these molecules inaccessible to Psh1 activity; however, the peri-CEN Cse4 pools are vulnerable to ubiquitin-mediated proteolysis. This dynamic property of Cse4 ubiquitination is important for mitosis, as the *pat1Δ* strain exhibits spindle checkpoint-dependent cell cycle delay and errors in chromosome segregation (Wang *et al.*, 1996; Haase *et al.*, 2013; Mishra *et al.*, 2013). Furthermore, we showed that ubiquitination of Cse4 is cell cycle regulated in wild-type cells. The abundance of ubiquitinated Cse4 increases from S phase to G2/M cells and decreases rapidly in cells synchronized in G1, suggesting a high degree of coordination between Cse4 ubiquitination and cell cycle. Future studies should give us insights into the functional relevance of the cell cycle-regulated ubiquitination of Cse4.

Cse4 is recruited to kinetochores in early S phase, and it remains stably associated with it throughout the cell cycle (Pearson *et al.*, 2004; Boeckmann *et al.*, 2013; Wisniewski *et al.*, 2014). These observations are supported by a low recovery of Cse4-GFP after photobleaching at metaphase kinetochores in a wild-type strain. ChIP assays and cell biology experiments have shown reduced levels of CEN-associated Cse4 in a *pat1Δ* strain, which were primarily attributed to the loss of peri-CEN Cse4 molecules from kinetochores (Haase *et al.*, 2013). It was unclear whether Pat1 is required for the recruitment of Cse4 molecules or its maintenance at kinetochores. Faster recovery of Cse4-GFP in *pat1Δ* strains indicates that Cse4 is exchanged rapidly at metaphase kinetochores. These results establish that Pat1 is not required for recruitment of Cse4 molecules to the CEN but is required for the stable maintenance of peri-CEN Cse4 molecules at kinetochores.

We propose that increased levels of ubiquitination of Cse4 in *pat1Δ* strains are contributed by an E3-ubiquitin ligase, Psh1. Support for this hypothesis is derived from results that showed 1) absence of Cse4 ubiquitination upon deletion of *PSH1* in a *pat1Δ* strain, 2) in vivo interaction of Pat1 with Psh1 and Cse4, and

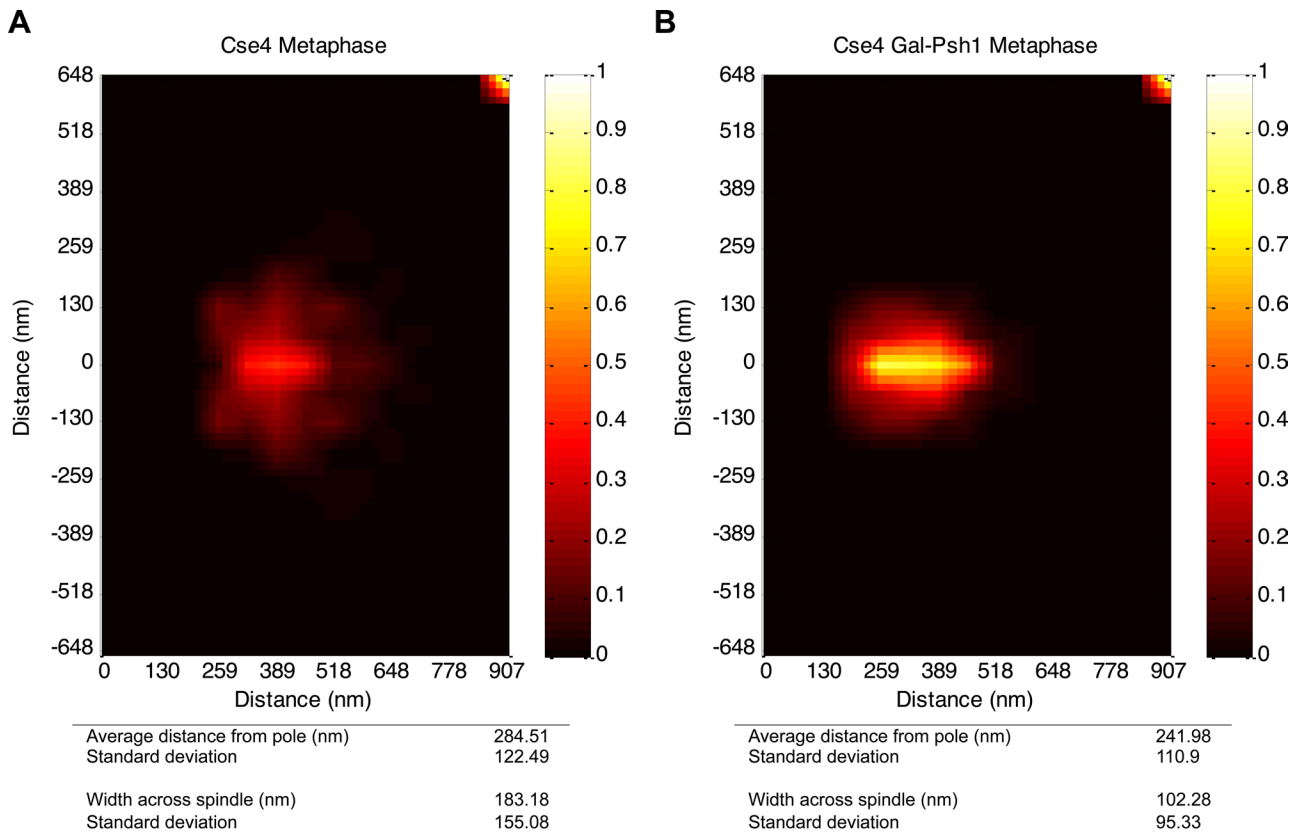


FIGURE 7: Induction of Psh1 causes structural alterations of Cse4 at kinetochores. Statistical probability map from experimental images representing kinetochore-associated Cse4 upon *PSH1* induction in a WT (KBY2012) strain. Statistical analysis of images is shown at the bottom. Distance from the spindle pole is the average distance. The width across the spindle is obtained by adding the average distances below and above the spindle axis. The detailed procedure used to prepare statistical probability maps was described previously (Haase *et al.*, 2013). (A) Experimental statistical probability map for Cse4 in a WT strain without *PSH1* induction. Map was generated from 208 images. (B) Experimental statistical probability map for Cse4 in a WT strain with *PSH1* induction (*GALPSH1*). Map was generated from 204 images.

3) increased levels of *CEN*-associated Psh1 in a *pat1Δ* strain during G2/M (mitotic cells), when maximum levels of Cse4 ubiquitination were observed. Further support for a role of Pat1 in regulating peri-*CEN* Cse4 is derived from our results with transient induction of *PSH1*, which resulted in phenotypes similar to a *pat1Δ* strain, such as increased ubiquitination and altered spatial distribution of Cse4.

In addition to regulating the levels of peri-*CEN* Cse4 (Haase *et al.*, 2013), we now provide evidence that Pat1 interacts with Scm3 and regulates its levels at the *CEN*. Scm3, a Cse4-specific chaperone, was shown to be involved in the protection of Cse4 from Psh1-mediated ubiquitination (Camahort *et al.*, 2007; Mizuguchi *et al.*, 2007; Stoler *et al.*, 2007; Hewawasam *et al.*, 2010; Mishra *et al.*, 2011; Shivaraju *et al.*, 2011). The *in vivo* interaction between Pat1 and Scm3 and the reduced levels of *CEN*-associated Scm3 in *pat1Δ* strains further support the role of Pat1 in the maintenance of Cse4 at the kinetochores. Unlike Cse4, which shows discrete localization to kinetochore clusters, localization of Scm3 is diffuse throughout the nucleus, and its association with centromeres is cell cycle dependent and dynamic (Luconi *et al.*, 2011; Mishra *et al.*, 2011; Wisniewski *et al.*, 2014). Hence it is not possible to use cell biology approaches similar to the ones used for Cse4 to discern the level of Scm3 in the peri-*CEN* and determine the relative contributions of Pat1 and Scm3 in Cse4 ubiquitination.

In conclusion, we showed that Pat1 plays a major role for peri-*CEN* Cse4 molecules to remain stably associated with the kinetochores. *CEN* chromatin-containing Pat1 shields Cse4 from Psh1-mediated ubiquitination to maintain kinetochore structure and function. In the absence of Pat1, these peri-*CEN* Cse4 molecules are vulnerable to Psh1-mediated ubiquitination. Our studies provide novel insights into how Pat1 helps to maintain peri-*CEN* Cse4 molecules at the budding yeast kinetochores.

MATERIALS AND METHODS

Strains, plasmids, and growth conditions

Yeast strains and plasmids used are listed in Table 1. Strains were grown in 1% yeast extract, 2% Bacto-Peptone, and 2% glucose (YPD) or in synthetic yeast medium containing either glucose (2%) or galactose plus raffinose (2% each) with supplements to allow for the selection of plasmids being examined. Wild-type strain with *cse4^{16KR}* (Au *et al.*, 2013) was grown in galactose plus raffinose (2% each) for 4 h to induce the expression of mutant allele of Cse4. Viability assays for the wild-type and *pat1Δ* strains containing *GALPSH1HA* (pMB1628) or vector (pRS426 *GAL1*) were carried out by spotting serial dilutions of equal numbers of cells from three independent transformants for each strain on synthetic medium at 30°C.

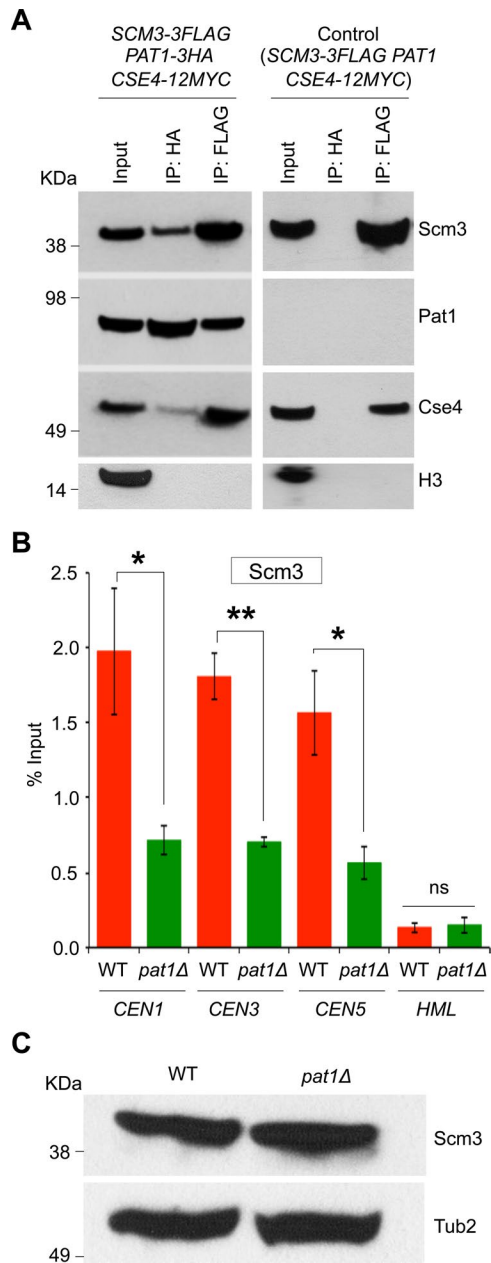


FIGURE 8: Pat1 interacts with Scm3, and *pat1Δ* strains showed reduced levels of centromeric Scm3. (A) Western blots of proteins copurifying with Pat1 and Scm3. Coimmunoprecipitation experiments were done using agarose beads conjugated with α -HA or α -Flag antibodies using cell extracts from strain (YMB7963) grown in YPD at 30°C expressing HA-tagged Pat1, Flag-tagged Scm3, and Myc-tagged Cse4 from their native promoters at the endogenous locus. A strain expressing Flag-tagged Scm3, Myc-tagged Cse4, and untagged Pat1 (JG595) from their native promoters at the endogenous locus was used for control experiments. Eluted proteins were analyzed by Western blotting with α -HA (Pat1), α -Flag (Scm3), α -Myc (Cse4), and α -H3 antibodies. (B) *CEN* association of Scm3 is reduced in *pat1Δ* strains. *CEN* levels of Scm3 were assayed by ChIP analysis of Scm3-Flag at *CEN* (*CEN1*, *CEN3*, and *CEN5*) and non-*CEN* (*HML*) DNA in WT (RC154) and *pat1Δ* (YMB8473) strains grown in YPD at 30°C. Enrichment was determined by qPCR and is shown as percentage input. Average from three biological experiments \pm SE. * $p < 0.05$, ** $p < 0.01$, Student's *t* test. (C) Expression of Scm3 is not affected in *pat1Δ* strains. Western blots showing protein levels of Scm3-Flag and Tub2 for strains used in B.

Cell cycle arrest and FACS analysis

Cells were grown in YPD to logarithmic phase at 30°C, treated for 2 h with 3 μ M α -factor (RP01002; GenScript, Piscataway, NJ) to arrest cells in G1, 0.2 M hydroxyurea (HU; H8627; Sigma-Aldrich, St. Louis, MO) to arrest cells in S phase, and 20 μ g/ml nocodazole (M1404; Sigma-Aldrich) to arrest cells in G2/M. Samples were analyzed by FACS to confirm the cell cycle arrest using a Becton-Dickinson FACSsort flow cytometer and Cell Quest software (BD Biosciences, Boston, MA). Cell cycle stages were determined based on nuclear position and cell morphology in propidium iodide-stained cells using the Zeiss Axioskop 2 microscope (Carl Zeiss, Peabody, MA) as described previously (Calvert and Lannigan, 2010).

Ubiquitin affinity pull-down assay

Ubiquitin affinity pull-down experiments were performed in three biological replicates as described previously (Hjerpe *et al.*, 2009; Au *et al.*, 2013). Briefly, yeast strains were grown to the logarithmic phase in YPD or synthetic medium with either 2% glucose or galactose plus raffinose (2% each) containing supplements to allow selection of plasmids being examined. Cultures were treated with sodium azide (0.1%) for 5 min, and cells were collected. Cell pellets were dissolved in lysis buffer (20 mM Na_2HPO_4 , 20 mM NaH_2PO_4 , 5 mM tetra-sodium pyrophosphate, 50 mM NaF, 1 mM dithiothreitol, 10 mM β -glycerophosphate, 2 mM EDTA, 1% NP-40, 5 mM *N*-ethylmaleimide, 1 mM phenylmethylsulfonyl fluoride) and protease inhibitor cocktail (P8215; Sigma-Aldrich), and an equal volume of glass beads (425–600 μ M) was added. Cells were lysed by bead beating (three times, 2 min each time), followed by vortexing for 60 min at 4°C. Cell lysates were normalized for protein concentration and used for affinity purification with 25 μ l of tandem ubiquitin-binding entities Agarose-TUBE1 (UM401; Life Sensors, Malvern, PA; exhibits high affinity to monoubiquitinated and polyubiquitin chain of K48 linkage) or control agarose (UM400; Life Sensors) at 4°C for 16 h. Beads were washed with 1 \times Tris-buffered saline (TBS) with Tween-20 (0.1%) at room temperature (three times, 5 min each time). The bound proteins were eluted in 2 \times Laemmli buffer by incubating at 100°C for 10 min and analyzed by Western blotting. Protein intensity signals were quantified using Gene Tools version 3.08 software (SynGene, Cambridge, United Kingdom). Relative ubiquitination of Cse4 in different cell cycle stages was measured as a ratio of ubiquitinated to input Cse4, and statistical significance was determined by Student's *t* test. We used an independent approach to confirm the results of ubiquitin affinity pull-down assays by performing immunoprecipitation of Cse4, followed by Western blotting as described previously (Ranjitkar *et al.*, 2010; Deyter and Biggins, 2014).

Immunoprecipitation, protein stability, and Western blotting assays

Immunoprecipitation experiments were performed as described previously (Mishra *et al.*, 2011). Protein samples were prepared using the trichloroacetic acid procedure (Cox *et al.*, 1997), protein concentrations were determined using the DC protein assay (Bio-Rad, Hercules, CA), and equal amounts of protein for each sample were assayed by Western blotting. Primary antibodies used were α -Myc (Z-5, sc-789; Santa Cruz Biotechnology, Dallas, TX), α -TAP (CAB1001; Thermo Scientific, Carlsbad, CA), α -HA (clone 12CA5; Roche, Pleasanton, CA), α -histone H3 (ab1791-100; Abcam, Cambridge, MA), α -histone H2B (ab1790; Abcam), α -Flag (F-3165; Sigma-Aldrich), α -ubiquitin (ab6309-1; Abcam), and α -tubulin 2 (Tub2; Mishra *et al.*, 2011). Secondary antibodies used were sheep α -mouse immunoglobulin (IgG; NA931V; Amersham Biosciences, Amersham, United Kingdom) and donkey α -rabbit IgG (NA934V, Amersham).

Saccharomyces cerevisiae strain	Genotype	Source or reference
BY4741	<i>MATa ura3Δ0 leu2Δ0 his3Δ1 met15Δ0</i>	Open Biosystems
YMB8126	<i>MATa his3Δ1 leu2Δ0 met15Δ0 ura3Δ0 PSH1-TAP::HIS3</i>	Open Biosystems
YMB9096	<i>MATa his3Δ1 leu2Δ0 met15Δ0 ura3Δ0 PSH1-TAP::HIS3 pat1Δ::URA3</i>	This study
YMB6398	<i>MATa ura3-52 lys2-801 ade2-101 trp1Δ63 his3Δ200 leu2Δ1 CSE4-13Myc::LEU2</i>	Au et al. (2008)
YMB8948	<i>MATa ura3-52 lys2-801 ade2-101 trp1Δ63 his3Δ200 leu2Δ1 CSE4-13Myc::LEU2 pat1Δ::TRP1</i>	This study
YMB8936	<i>MATa ura3-1 leu2,3-112 his3-1 trp1-1 ade2-1 can1-100 Δbar1 CSE4-12Myc::URA3 SCM3-3Flag::kanMX pat1Δ::TRP1</i>	This study
YMB8422	<i>MATa ura3-52 lys2-801 ade2-101 trp1Δ63 his3Δ200 leu2Δ1 CSE4-13Myc::LEU2 pat1Δ::URA3</i>	This study
KBY2012	<i>MATa trp1Δ63 leu2Δ ura3-52 his3 Δ 200 lys2-8Δ1 CSE4GFP::TRP1 (pKK1) SPC29CFP::KAN</i>	Haase et al. (2013)
KBY8166	<i>MATa trp1Δ63 leu2Δ ura3-52 his3Δ200 lys2-8Δ1 CSE4GFP::TRP1 (pKK1) SPC29CFP::KAN pat1Δ::NAT</i>	Haase et al. (2013)
KBY8116	<i>MATa trp1Δ63 leu2Δ ura3-52 his3Δ200 lys2-8Δ1 NDC80GFP::KAN SPC29RFP::Hg</i>	Haase et al. (2013)
YMB9280	<i>MATa his3Δ1 leu2Δ0 met15Δ0 ura3Δ0 PSH1-TAP::HIS3 PAT1-FLAG::URA3</i>	This study
YMB9281	<i>MATa his3Δ1 leu2Δ0 met15Δ0 ura3Δ0 PSH1-TAP::HIS3 CSE4HA::NAT</i>	This study
YMB9282	<i>MATa his3Δ1 leu2Δ0 met15Δ0 ura3Δ0 PSH1-TAP::HIS3 CSE4HA::NAT pat1Δ::URA3</i>	This study
YMB9311	<i>MATa ura3-52 lys2-801 ade2-101 trp1Δ63 his3Δ200 leu2Δ1 CSE4-13Myc::LEU2 psh1Δ::KAN</i>	This study
YMB9312	<i>MATa ura3-52 lys2-801 ade2-101 trp1Δ63 his3Δ200 leu2Δ1 CSE4-13Myc::LEU2 psh1Δ::KAN pat1Δ::URA3</i>	This study
RC154	<i>MATa ura3-1 leu2,3-112 his3-1 trp1-1 ade2-1 can1-100 Δbar1 SCM3-3Flag::KAN NDC10-13Myc::TRP1</i>	Camahort et al. (2007)
YMB8473	<i>MATa ura3-1 leu2,3-112 his3-1 trp1-1 ade2-1 can1-100 Δbar1 SCM3-3Flag::KAN NDC10-13Myc::TRP1 pat1Δ::URA3</i>	This study
YMB7963	<i>MATa ura3-1 leu2,3-112 his3-1 trp1-1 ade2-1 can1-100 Δbar1 CSE4-12Myc::URA3 SCM3-3Flag::KAN PAT1-3HA::TRP1</i>	This study
JG595	<i>MATa ura3-1 leu2,3-112 his3-1 trp1-1 ade2-1 can1-100 Δbar1 PAT1 CSE4-12Myc::URA3 SCM3-3Flag::kanMX</i>	Camahort et al. (2007)
YPH499	<i>MATa ura3-52 lys2-801 ade2-101 trp1Δ63 his3Δ200 leu2Δ1</i>	Sikorski and Hieter (1989)

Plasmid	Description	Reference
pRS426-GAL1	2μm URA3 GAL1	Sikorski and Hieter (1989), Mumberg et al. (1994)
pMB1628	2μm URA3 GAL1/10-PSH1-HA	Gelperin et al. (2005)

TABLE 1: Strains and plasmids used in this study.

Protein stability assays were performed as described previously (Au et al., 2008; Au et al., 2013).

Chromatin immunoprecipitation and quantitative PCR

ChIP experiments were carried out in three biological replicates as described previously (Mishra et al., 2007, 2011), with minor modifications. Briefly, cultures were cross-linked with 1% formaldehyde (final concentration) for 15 min and quenched with 125 mM glycine for 5 min at room temperature. Cell pellets were collected by centrifugation, washed with TBS (20 mM Tris-HCl, pH 7.6; 150 mM NaCl) and then used to prepare spheroplasts using Zymolyase 100T. Spheroplasts were washed once with postspheroplasting buffer (1.2 M sorbitol, 1 mM MgCl₂, 20 mM Na-1,4-piperazinediethanesulfonic

acid, pH 6.8), followed by three washes with FA buffer (50 mM Na-HEPES, pH 7.6, 1 mM EDTA, 1% Triton X-100, 150 mM NaCl, 0.1% Na-deoxycholate) with protease inhibitor cocktail (P8215; Sigma-Aldrich). Spheroplasts were then resuspended in FA buffer with protease inhibitors and sonicated on ice at 30% output cycle for five 12-s bursts applied 2 min apart to obtain an average DNA fragment size of 400 base pairs. The resulting soluble chromatin fraction was used for immunoprecipitation experiments as described previously (Mishra et al., 2007, 2011), using the following antibodies: α-TAP (CAB1001; Thermo Scientific), α-Myc (A7470; Sigma-Aldrich), α-Flag (A2220; Sigma-Aldrich), and α-glutathione-S-transferase (Z-5, sc-459; Santa Cruz Biotechnology). Quantitative-PCR using ChIP DNA (ChIP-qPCR) was performed in the 7500 Fast Real Time PCR System using Fast

Locus	Forward (5'-3')	Reverse (5'-3')	Reference
<i>CEN1</i>	CTCGATTTCATAAGTGTGCC	GTGCTTAAGAGTTCTGTACCAC	Choy et al. (2011)
<i>CEN3</i>	GATCAGCGCCAAACAATATGG	AACTCCACCAGTAAACGTTTC	Choy et al. (2011)
<i>CEN5</i>	AAGAACTATGAATCTGTAAATGACTGATTCAAT	CTTGCACTAAACAAGACTTTATACTACGTTTATG	Choy et al. (2011)
<i>ACT1</i>	AATGGCGTGAGGTAGAGAGAAACC	ACAACGAATTGAGAGTTGCCCCAG	Au et al. (2008)
<i>HML</i>	CACAGCGGTTTCAAAAAAGCTG	GGATTTTATTTAAAAATCGAGAGG	Choy et al. (2011)
<i>CEN3-DraI</i>	TTGATGAACTTTTCAAAGATGAC	GTCAACGAGTCTCTCTGGCTA	Mishra et al. (2013)
<i>ADP1-DraI</i>	ATCCAAATGTGCTCAAGATAGTAGC	CACCAAACAACATTTACTAGCAGTG	Mishra et al. (2013)

TABLE 2: Primers used in this study.

SYBR Green Master Mix (Applied Biosystems, Foster City, CA) following conditions described in Mishra et al. (2011). The enrichment values were calculated as percentage input using the $\Delta\Delta C_t$ method (Livak and Schmittgen, 2001). The primer sequences used in this study are listed in Table 2.

Preparation of yeast nuclei and *DraI* accessibility assay

Wild-type and *pat1Δ* strains carrying vector (pRS426 *GAL1*) or *GALPSH1HA* (pMB1628) were grown in synthetic yeast medium with galactose plus raffinose (2% each) for 6 h at 30°C to mid log phase. Nuclei were prepared from the cells, digested with *DraI* (0 and 100 U/ml of nuclei) for 30 min at 37°C, and DNA was extracted following the procedure described in previous studies (Saunders et al., 1990; Mishra et al., 2013). The susceptibility of chromatin to *DraI* digestion (100 U/ml) was determined by quantitative real-time PCR as described previously (Mishra et al., 2013) using primers flanking *DraI* sites of *CEN3* (*CEN*-chromatin) and *ADP1* (non-*CEN* chromatin used as a control). The fraction of DNA digested by the *DraI* (100 U/ml) enzyme was determined by normalizing the *Ct* values to an untreated control (no *DraI*).

Imaging techniques and microscopy

Cultures grown to logarithmic phase at room temperature were used for all imaging experiments. Metaphase cells were selected based on the position of kinetochores (*Cse4*-GFP) and spindle pole bodies (*Spc29*-CFP) as live-cell markers (Chen et al., 2000; Maddox et al., 2000). Cells were imaged at room temperature on a Nikon TE-2000E inverted microscope equipped with a 1.4 numerical aperture, 100× Plan-Apo objective (Nikon Instruments, Melville, NY) as described previously (Salmon et al., 2013). Thirteen images stepped through a 200-nm z-axis were obtained for each cell using imaging and acquisition software from MetaMorph (Molecular Devices, Sunnyvale, CA). Kinetochores were measured by fitting to a Gaussian distribution to the fluorescent spot. The width of the fluorescent spot was determined from the full-width, full-maximum of the Gaussian distribution. The detailed experimental procedure for the preparation of statistical probability maps was described previously (Haase et al., 2013).

Cse4-GFP FRAP experiments were done using cells grown to logarithmic phase of growth at room temperature and imaging of metaphase cells as described previously (Chen et al., 2000; Maddox et al., 2000). The positions of kinetochores (*Cse4*-GFP) and spindle pole bodies (*Spc29*-CFP) were used as live-cell markers for cell cycle stage to identify cells in metaphase. One cluster of *Cse4*-GFP fluorescence was photobleached with a short, 35-ms exposure of focused 488-nm laser light in metaphase cells. A five-plane fluorescence z-series (0.5- μ m steps) was obtained immediately after laser exposure to measure the fluorescence photobleaching and recovery as previously described (Pearson et al., 2004). *Cse4*-GFP fluorescence intensities were determined by collecting the integrated

intensity by placing a 5 × 5-pixel region around the localized fluorescence. The total *Cse4*-GFP fluorescence intensity was then determined by subtracting the intracellular background levels.

ACKNOWLEDGMENTS

We thank Jennifer Gerton, Sue Biggins, Roy Parker, Michael Lichten, and Richard Baker for reagents, Kathy McKinnon of the National Cancer Institute Vaccine Branch FACS Core for assistance with FACS, Wei-Chun Au for assistance with the ubiquitin pull-down assay, and members of the Basrai laboratory for discussions. Support for P.K.M., L.E.D., and M.A.B. was provided by the Intramural Research Program of the National Cancer Institute, National Institutes of Health. Support for J.G., J.H., E.Y., and K.B. was derived from National Institute of Health Grant R37 GM32238 to K.B.

REFERENCES

- Allshire RC, Karpen GH (2008). Epigenetic regulation of centromeric chromatin: old dogs, new tricks? *Nat Rev Genet* 9, 923–937.
- Au WC, Crisp MJ, DeLuca SZ, Rando OJ, Basrai MA (2008). Altered dosage and mislocalization of histone H3 and *Cse4p* lead to chromosome loss in *Saccharomyces cerevisiae*. *Genetics* 179, 263–275.
- Au WC, Dawson AR, Rawson DW, Taylor SB, Baker RE, Basrai MA (2013). A novel role of the N-terminus of budding yeast histone H3 variant *Cse4* in ubiquitin-mediated proteolysis. *Genetics* 194, 513–518.
- Bloom KS, Carbon J (1982). Yeast centromere DNA is in a unique and highly ordered structure in chromosomes and small circular minichromosomes. *Cell* 29, 305–317.
- Boeckmann L, Takahashi Y, Au WC, Mishra PK, Choy JS, Dawson AR, Szeto MY, Waybright TJ, Heger C, McAndrew C, et al. (2013). Phosphorylation of centromeric histone H3 variant regulates chromosome segregation in *S. cerevisiae*. *Mol Biol Cell* 24, 2034–2044.
- Burrack LS, Berman J (2012). Flexibility of centromere and kinetochore structures. *Trends Genet* 28, 204–212.
- Calvert ME, Lannigan J (2010). Yeast cell cycle analysis: combining DNA staining with cell and nuclear morphology. *Curr Protoc Cytom Chapter 9: Unit 9.32.1–16*.
- Camahort R, Li B, Florens L, Swanson SK, Washburn MP, Gerton JL (2007). *Scm3* is essential to recruit the histone h3 variant *cse4* to centromeres and to maintain a functional kinetochore. *Mol Cell* 26, 853–865.
- Chen Y, Baker RE, Keith KC, Harris K, Stoler S, Fitzgerald-Hayes M (2000). The N terminus of the centromere H3-like protein *Cse4p* performs an essential function distinct from that of the histone fold domain. *Mol Cell Biol* 20, 7037–7048.
- Cho US, Corbett KD, Al-Bassam J, Bellizzi JJ 3rd, De Wulf P, Espelin CW, Miranda JJ, Simons K, Wei RR, Sorger PK, Harrison SC (2010). Molecular structures and interactions in the yeast kinetochore. *Cold Spring Harb Symp Quant Biol* 75, 395–401.
- Choy JS, Acuna R, Au WC, Basrai MA (2011). A role for histone H4K16 hypoacetylation in *Saccharomyces cerevisiae* kinetochore function. *Genetics* 189, 11–21.
- Choy JS, Mishra PK, Au WC, Basrai MA (2012). Insights into assembly and regulation of centromeric chromatin in *Saccharomyces cerevisiae*. *Biochim Biophys Acta* 1819, 776–783.
- Clarke L, Carbon J (1980). Isolation of a yeast centromere and construction of functional small circular chromosomes. *Nature* 287, 504–509.

- Collins KA, Furuyama S, Biggins S (2004). Proteolysis contributes to the exclusive centromere localization of the yeast Cse4/CENP-A histone H3 variant. *Curr Biol* 14, 1968–1972.
- Cox JS, Chapman RE, Walter P (1997). The unfolded protein response coordinates the production of endoplasmic reticulum protein and endoplasmic reticulum membrane. *Mol Biol Cell* 8, 1805–1814.
- Crotti LB, Basrai MA (2004). Functional roles for evolutionarily conserved Spt4p at centromeres and heterochromatin in *Saccharomyces cerevisiae*. *EMBO J* 23, 1804–1814.
- Deyter GM, Biggins S (2014). The FACT complex interacts with the E3 ubiquitin ligase Psh1 to prevent ectopic localization of CENP-A. *Genes Dev* 28, 1815–1826.
- Gelperin DM, White MA, Wilkinson ML, Kon Y, Kung LA, Wise KJ, Lopez-Hoyo N, Jiang L, Piccirillo S, Yu H, et al. (2005). Biochemical and genetic analysis of the yeast proteome with a movable ORF collection. *Genes Dev* 19, 2816–2826.
- Gonen S, Akiyoshi B, Iadanza MG, Shi D, Duggan N, Biggins S, Gonen T (2012). The structure of purified kinetochores reveals multiple microtubule-attachment sites. *Nat Struct Mol Biol* 19, 925–929.
- Haase J, Mishra PK, Stephens A, Haggerty R, Quammen C, Taylor RM 2nd, Yeh E, Basrai MA, Bloom K (2013). A 3D map of the yeast kinetochore reveals the presence of core and accessory centromere-specific histone. *Curr Biol* 23, 1939–1944.
- Hartzog GA, Basrai MA, Ricupero-Hovasse SL, Hieter P, Winston F (1996). Identification and analysis of a functional human homolog of the SPT4 gene of *Saccharomyces cerevisiae*. *Mol Cell Biol* 16, 2848–2856.
- Hewawasam GS, Mattingly M, Venkatesh S, Zhang Y, Florens L, Workman JL, Gerton JL (2014). Phosphorylation by casein kinase 2 facilitates Psh1 protein-assisted degradation of Cse4 protein. *J Biol Chem* 289, 29297–29309.
- Hewawasam G, Shivaraju M, Mattingly M, Venkatesh S, Martin-Brown S, Florens L, Workman JL, Gerton JL (2010). Psh1 is an E3 ubiquitin ligase that targets the centromeric histone variant Cse4. *Mol Cell* 40, 444–454.
- Hjerpe R, Aillet F, Lopitz-Otsoa F, Lang V, England P, Rodriguez MS (2009). Efficient protection and isolation of ubiquitylated proteins using tandem ubiquitin-binding entities. *EMBO Rep* 10, 1250–1258.
- Jacobs CW, Adams AE, Szanislo PJ, Pringle JR (1988). Functions of microtubules in the *Saccharomyces cerevisiae* cell cycle. *J Cell Biol* 107, 1409–1426.
- Kitagawa K, Hieter P (2001). Evolutionary conservation between budding yeast and human kinetochores. *Nat Rev Mol Cell Biol* 2, 678–687.
- Lampert F, Westermann S (2011). A blueprint for kinetochores—new insights into the molecular mechanics of cell division. *Nat Rev Mol Cell Biol* 12, 407–412.
- Lawrimore J, Bloom KS, Salmon ED (2011). Point centromeres contain more than a single centromere-specific Cse4 (CENP-A) nucleosome. *J Cell Biol* 195, 573–582.
- Lechner J, Carbon J (1991). A 240 kd multisubunit protein complex, CBF3, is a major component of the budding yeast centromere. *Cell* 64, 717–725.
- Livak KJ, Schmittgen TD (2001). Analysis of relative gene expression data using real-time quantitative PCR and the 2(-Delta Delta C(T)) method. *Methods* 25, 402–408.
- Luconi L, Araki Y, Erlemann S, Schiebel E (2011). The CENP-A chaperone Scm3 becomes enriched at kinetochores in anaphase independently of CENP-A incorporation. *Cell Cycle* 10, 3369–3378.
- Maddox PS, Bloom KS, Salmon ED (2000). The polarity and dynamics of microtubule assembly in the budding yeast *Saccharomyces cerevisiae*. *Nat Cell Biol* 2, 36–41.
- Maddox PS, Corbett KD, Desai A (2012). Structure, assembly and reading of centromeric chromatin. *Curr Opin Genet Dev* 22, 139–147.
- Meluh PB, Yang P, Glowczewski L, Koshland D, Smith MM (1998). Cse4p is a component of the core centromere of *Saccharomyces cerevisiae*. *Cell* 94, 607–613.
- Meraldi P, McAinsh AD, Rheinbay E, Sorger PK (2006). Phylogenetic and structural analysis of centromeric DNA and kinetochore proteins. *Genome Biol* 7, R23.
- Mishra PK, Au WC, Choy JS, Kuich PH, Baker RE, Foltz DR, Basrai MA (2011). Misregulation of Scm3p/HJURP causes chromosome instability in *Saccharomyces cerevisiae* and human cells. *PLoS Genet* 7, e1002303.
- Mishra PK, Baum M, Carbon J (2007). Centromere size and position in *Candida albicans* are evolutionarily conserved independent of DNA sequence heterogeneity. *Mol Genet Genomics* 278, 455–465.
- Mishra PK, Ottmann AR, Basrai MA (2013). Structural integrity of centromeric chromatin and faithful chromosome segregation requires Pat1. *Genetics* 195, 369–379.
- Mizuguchi G, Xiao H, Wisniewski J, Smith MM, Wu C (2007). Nonhistone Scm3 and histones CenH3-H4 assemble the core of centromere-specific nucleosomes. *Cell* 129, 1153–1164.
- Mumberg D, Muller R, Funk M (1994). Regulatable promoters of *Saccharomyces cerevisiae*: comparison of transcriptional activity and their use for heterologous expression. *Nucleic Acids Res* 22, 5767–5768.
- Mythreye K, Bloom KS (2003). Differential kinetochore protein requirements for establishment versus propagation of centromere activity in *Saccharomyces cerevisiae*. *J Cell Biol* 160, 833–843.
- Pearson CG, Yeh E, Gardner M, Odde D, Salmon ED, Bloom K (2004). Stable kinetochore-microtubule attachment constrains centromere positioning in metaphase. *Curr Biol* 14, 1962–1967.
- Pot I, Measday V, Snydsman B, Cagney G, Fields S, Davis TN, Muller EG, Hieter P (2003). Chl4p and iml3p are two new members of the budding yeast outer kinetochore. *Mol Biol Cell* 14, 460–476.
- Przewlorka MR, Glover DM (2009). The kinetochore and the centromere: a working long distance relationship. *Annu Rev Genet* 43, 439–465.
- Ranjitkar P, Press MO, Yi X, Baker R, MacCoss MJ, Biggins S (2010). An E3 ubiquitin ligase prevents ectopic localization of the centromeric histone H3 variant via the centromere targeting domain. *Mol Cell* 40, 455–464.
- Salmon ED, Shaw SL, Waters JC, Waterman-Storer CM, Maddox PS, Yeh E, Bloom K (2013). A high-resolution multimode digital microscope system. *Methods Cell Biol* 114, 179–210.
- Saunders MJ, Yeh E, Grunstein M, Bloom K (1990). Nucleosome depletion alters the chromatin structure of *Saccharomyces cerevisiae* centromeres. *Mol Cell Biol* 10, 5721–5727.
- Schneider CA, Rasband WS, Eliceiri KW (2012). NIH Image to ImageJ: 25 years of image analysis. *Nat Methods* 9, 671–675.
- Scott KC, Bloom KS (2014). Lessons learned from counting molecules: how to lure CENP-A into the kinetochore. *Open Biol* 4, 140191.
- Shivaraju M, Camahort R, Mattingly M, Gerton JL (2011). Scm3 is a centromeric nucleosome assembly factor. *J Biol Chem* 286, 12016–12023.
- Sikorski RS, Hieter P (1989). A system of shuttle vectors and yeast host strains designed for efficient manipulation of DNA in *Saccharomyces cerevisiae*. *Genetics* 122, 19–27.
- Stoler S, Rogers K, Weitze S, Morey L, Fitzgerald-Hayes M, Baker RE (2007). Scm3, an essential *Saccharomyces cerevisiae* centromere protein required for G2/M progression and Cse4 localization. *Proc Natl Acad Sci USA* 104, 10571–10576.
- Verdaasdonk JS, Bloom K (2011). Centromeres: unique chromatin structures that drive chromosome segregation. *Nat Rev Mol Cell Biol* 12, 320–332.
- Wang X, Watt PM, Louis EJ, Borts RH, Hickson ID (1996). Pat1: a topoisomerase II-associated protein required for faithful chromosome transmission in *Saccharomyces cerevisiae*. *Nucleic Acids Res* 24, 4791–4797.
- Weinert TA, Kiser GL, Hartwell LH (1994). Mitotic checkpoint genes in budding yeast and the dependence of mitosis on DNA replication and repair. *Genes Dev* 8, 652–665.
- Wisniewski J, Hajj B, Chen J, Mizuguchi G, Xiao H, Wei D, Dahan M, Wu C (2014). Imaging the fate of histone Cse4 reveals de novo replacement in S phase and subsequent stable residence at centromeres. *Elife*, e02203.
- Yu Y, Srinivasan M, Nakanishi S, Leatherwood J, Shilatfard A, Sternglanz R (2011). A conserved patch near the C terminus of histone H4 is required for genome stability in budding yeast. *Mol Cell Biol* 31, 2311–2325.